DYNA
http://dyna.medellin.unal.edu.co/

UNIVERSIDAD NACIONAL DE COLOMBIA

Microstructure influence on crack propagation behavior of nodular cast iron

Carla Tatiana Mota Anflor, José David Hurtado-Agualimpia, Adrián Alberto Betancur-Arroyave, Sergio Henrique da Silva Carneiro & Jhon Nero Vaz Goulart

Group of Experimental and Computational Mechanics, University of Brasilia, Campus Gama, Brazil
anflor@unb.br, jodaha@hotmail.com, aabetanc@gmail.com, shscarneiro@gmail.com, jvazgoulart@gmail.com

Received: November 25th, 2024. Received in revised form: May 19th, 2025. Accepted: July 25th, 2025.

Abstract
This paper offers a comprehensive analysis of the crack propagation behavior of a specific type of Nodular Cast Iron (NCI) and its correlation with microstructural morphology. To estimate da/dN vs K curves, crack propagation tests were conducted utilizing Compact Test Specimens (CTS). Additionally, Scanning Electron Microscopy Analysis was employed to characterize the microstructure morphology on the surfaces of the fractured specimens, with specific attention to the size and distribution of graphite nodules within the ferritic matrix. The findings of the study suggest that the position from which the CTS is extracted is contingent upon the graphite distribution, which could have a noteworthy impact on the crack propagation behavior of the investigated NCI alloy.

Keywords: nodular cast iron; fracture mechanics; scanning electron microscopy; micrographic analysis

Influencia de la microestructura en el comportamiento de propagación de grietas en fundición nodular

Resumen
Este artículo ofrece un análisis exhaustivo del comportamiento de propagación de grietas de un tipo específico de fundición nodular (NCI) y su correlación con la morfología microestructural. Para estimar las curvas da/dN vs K, se realizaron pruebas de propagación de grietas utilizando muestras de prueba compactas (CTS). Además, se empleó análisis de microscopía electrónica de barrido para caracterizar la morfología de la microestructura en las superficies de las muestras fracturadas, con atención específica al tamaño y la distribución de los nódulos de grafito dentro de la matriz ferrítica. Los hallazgos del estudio sugieren que la posición desde la cual se extrae el CTS depende de la distribución del grafito, lo que podría tener un impacto notable en el comportamiento de propagación de grietas de la aleación NCI investigada.

Palabras claves: fundición nodular; mecanismos de fractura; microscopia electrónica de barrido; análisis micrográfico.

1. Introduction

Nodular Cast Iron (NCI) finds widespread usage in various engineering applications owing to its favorable combination of mechanical properties, including good fatigue strength, high machinability, and ductility. The chemical composition, particularly the presence of nickel, copper, and molybdenum, endows this material with desirable mechanical properties suited for diverse industrial applications. Initially introduced in 1948, NCI is characterized as a ternary Fe-C-Si alloy with proportions typically ranging from 3.5% to 3.9% for carbon and 1.8% to 2.8% for silicon [1]. Some authors also refer to NCI as Ductile Cast Iron (DCI) due to its ductile behavior [2-5], or alternatively as Spheroidal Graphite Cast Iron (SGI) [6-9] due to the manner in which the graphite nucleates. The main microstructural feature of NCI is the formation of spheroidal graphite, commonly referred to as nodules, which directly influences the physical properties of the material. NCI is

How to cite: Anflor, C.T.M., Hurtado-Agualimpia, J.D., Betancur-Arroyave, A.A., Carneiro, S.H.de S., and Goulart J.N.V., Microstructure influence on crack propagation behavior of nodular cast iron. DYNA, (92)238, pp. 93-102, July - September, 2025.

typically characterized by a high strength-to-weight ratio, excellent fatigue strength, high machinability, and distinctive ductile behavior, making it widely utilized in the manufacturing of various mechanical components such as manifolds, crankshafts, wheels, and gears [2,10]. These attractive characteristics are attributed to several parameters that significantly affect the mechanical properties, including the influence of manganese and copper. These elements stabilize pearlite, facilitate graphite formation, enhance strength, and improve the material's ability to withstand cyclic loads [8]. A wealth of studies has delved into the behavior of NCI, encompassing diverse topics such as: the dispersion of NCI's mechanical properties and their implications [11], analyses of matrix phase composition in fracture mechanics [12,13], the impact of graphite morphology on mechanical properties [8], micromechanical failures under impact, static, and fatigue stress [14], as well as investigations into fracture under dynamic loading [8], among other notable studies. According to [15], NCI can exhibit various structures including ferritic, pearlitic, austenitic, or intermediate structures, which depend on the chemical composition of the matrix and the applied heat treatment. NCI typically features spheroidal graphite embedded in a ferritic-pearlitic, pearlitic, or ferritic matrix, with each matrix phase composition impacting the material's behavior differently [12,16]. In addition to the significance of the cast iron matrix phase, certain characteristics of graphite nodules are equally important and extensively studied. Parameters such as the size, roundness, shape, and distribution of graphite nodules can significantly influence the performance of NCI, particularly under dynamic loading conditions [17-19]. A thorough understanding of the mechanisms involved in the spheroidization of graphite has been the subject of study for many researchers [20-22]. According to these studies, graphite nodule flotation is caused by excessive growth of certain nodules, which absorb carbon directly from the liquid. Due to their lower density, graphite nodules tend to float to the surface, a phenomenon that is more pronounced in thick sections or under slow cooling rates, resulting in inferior mechanical properties. Various articles have reported graphite flotation through metallographic analysis ([6] and [23,24]). In the field of fracture mechanics for nodular irons, previous studies were conducted under the assumption that graphite nodules had a negligible effect on the fracture mechanism. Many works in fracture mechanics were carried out on nodular cast iron, where graphite nodules were considered to have an almost negligible effect on the fracture mechanism [25-27], as the material was viewed as porous due to the low resistance of graphite. However, recent research has focused on analyzing the influence of these graphite nodules [28]. Studies have investigated failure micromechanisms in nodular cast iron under various loading conditions, including cyclic loading generating fatigue and the crack propagation process [29]. According to [30], the resistance of nodular cast iron to propagation and fatigue cracking is strongly influenced by the matrix, graphite morphological particles, and load conditions.

The same authors show in their work the influence of factors such as the stress ratio (R), the detachment of the graphite nodules, the cleavage of the ferritic shield. Other authors such as [31], highlight the importance of graphite nodules and the microstructure depending on the NCI matrix. For example, considering a tensile stress condition, the possible influence on the graphite nodules will depend on the type of matrix it is part of, if the matrix is completely ferritic there will be little influence of the nucleation processes and secondary crack growth inside the nodules. The microstructure influence on fatigue crack propagation NCI with different volume fractions of ferrite and pearlite for a set of samples have been also considered [32] following the ASTM E647 standard with load ratio R equals to 0.1, 0.5 and 0.75. NCI fatigue crack propagation resistance is strongly affected by the graphite nodulization and by the phase distribution (taking an important role for higher R or ΔK) within the microstructures. The fatigue crack propagation micromechanics in a ferritic NCI was done by means of scamming electron microscope (SEM) and digital microscope (DM) observations by [33] to observe the graphite influence over ferritic matrix during the fracture process, and he found that for low values of ΔK and R the material did not behave in relation to homogeneous material and suggested that for high values of ΔK or R a representative plastic zone could be generated.

According to the authors the fatigue crack propagation inside the graphite nodules was affected by the presence of a mechanical property gradient inside the graphite nodules. The mechanical gradient presented with the graphite perhaps resulted from the nodule solidification and growth mechanisms. It is also important to mention that in this work some considerations regarding the parameter K were underlined based on the experimental results. The fatigue crack propagation resistance for a ferritic NCI with degenerate nodules and compared the material behavior obtained to commercial ferritic NCIs were investigated by [34,35]. For this case the Pari's modelwas used [35]. In that work, the morphology and the reasons that can degenerate the graphite nodules were listed, such as, the presence of carbides, chunky graphite due to excess of rare earth additions, exploded graphite resulting from the excess of rare earth presence, compacted graphite due to low residual magnesium and/or rare earth, Graphite flotation, which potential causes can be high carbon equivalent, excess of pouring temperature, slow cooling rate in thicker sections or an insufficient inoculation, among others. Based on the analysis performed, the authors concluded that the presence of degenerated graphite influenced the crack propagation micromechanics but didn't affect the mechanical properties with respect to the resistance.

The main goal of this work is to give continuity of a comprehensive numerical and experimental characterization of nodular cast iron performed on the same batch of samples previously studied in [36,37] and [11]. In this sense the efforts turn to determine the material behavior when submitted to fatigue crack growth. The present batch of NCI presents in its morphology nearly spherical inclusions of graphite embedded in a homogeneous ferritic matrix. Depending on the graphite distribution as well as their morphology, the crack growth rate can be influenced significantly and additional tests (micrographic analyses and scanning electron microscopy equipped with energy-dispersive X-ray (SEM-EDX) analysis) are used in the

fractured specimens to support the discussions. This paper is organized as follows. Section 2 introduces the methodology employed for manufacturing of the fracture specimens, the procedure for performing the fracture tests, the Scanning Electron Microscopy analysis and the micrographic analysis. The experimental results obtained from fracture tests and the evaluations of the microstructures aspect are presented in section 3. Finally, the conclusions are presented and discussed in section 4.

2. Materials and methods

2.1 Specimens

Specimens were fabricated from a $50 \times 50 \times 300$ mm nodular cast iron block without undergoing heat treatment. Fig.1(a) illustrates the orientations of each type of specimen, while Fig.1 (b) depicts the dimensions according to ASTM E647 standards. Although the microstructure of NCI lacks patterns akin to those found in laminated metals, certain specimens were extracted in alternative orientations to assess fracture toughness concerning graphite nodule distribution. As noted by [21], during the cooling process, graphite, being less dense, tends to migrate towards the upper surface. Consequently, there arose a necessity to analyze the influence of crack propagation in volume elements exhibiting variations in nodular density. Moreover, it is essential to highlight that production in cast condition is influenced by the cooling rate within the mold and the wall thicknesses of the cast part. Hence, the tests will be conducted with consideration given to the position of each sample within the NCI block.

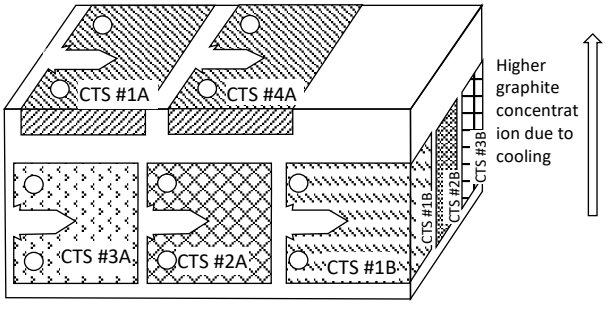

(a)

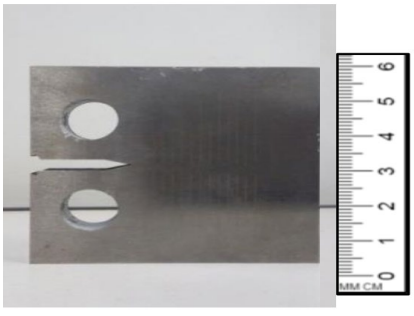

(b)

Figure 1. Details of the specimens: (a) block removal location (b) Specimen geometry.
Source: Own elaboration

2.2 Tensile

Due to the foundry process, nodular cast irons exhibit a wide range of mechanical properties. Various factors influence the mechanical properties of NCI, including cooling rate, chemical composition, graphite morphology, and their distribution, among others. For conducting the tests, the INSTRON 8801 universal testing machine was utilized. To furnish additional insights into the NCI under investigation, stress-strain relationships were determined through tensile testing.

2.3 Fatigue crack growth rate testing

For the fracture test, an MTS 810 machine was utilized, where seven CTS (ASTM) specimens with a thickness of 12mm were tested. The load ratio was set to R= Pmin/Pmax = 0.1, maintaining a constant load amplitude, and a sinusoidal loading waveform was applied with a frequency of 30 Hz throughout the test. The da/dN curve data were acquired and recorded for each specimen. To monitor crack growth, an MTS model 632.02 strain gauge was positioned at the opening of the specimen. Following the pre-crack propagation of the CTS, fatigue crack propagation tests were conducted to obtain the K_C and K_{th} values of the da/dN versus ΔK curve for the NCI. Therefore, K_{IC} values from the literature for NCI were employed. The tests adhered to ASTM E647 standard recommendations for crack growth with controlled K. The test procedures included constant load amplitude tests with increasing K and decreasing K tests, aiming to obtain stages I, II, and III for the NCI.

2.3.1. Test with constant load amplitude and increasing K

To conduct this test, ASTM E647 standard recommends maintaining a rising K to obtain a suitable crack growth rate for measuring the Paris curve parameters. The crack growth rate should exceed 10^{-5} mm/cycle, as lower rates may pose challenges regarding fatigue pre-crack considerations. It is advised to maintain a constant load amplitude (ΔP) and fixed stress ratio (R) and frequency (ω) throughout the test. Therefore, for three (CTS #1A, CTS #2A, CTS #3A, and CTS #4A, CTS #1B) of the four CTSs used for the crack propagation tests with increasing K, the same values of ΔP = 7.94kN were applied for each parameter, with an initial ΔK of approximately 12 MPa$\sqrt{m}$. CTS #2A was the only case where a smaller load (ΔP = 6.55 kN) was utilized.

2.3.2. Decreasing K test

During this type of test, the loading amplitude decreases until reaching a negative gradient of K. The aim of such tests is to determine the value of ΔK_{th}. To achieve this, it is necessary to define a $K_{máx}$, from which point ΔK is decreased until a value is reached where crack growth becomes negligible. For the calculation of ΔK_{th}, a linear regression of the logarithm of da/dN versus the logarithm of ΔK is applied using at least five equally spaced points on the curve between 10^{-6} and 10^{-7}mm/cycle. The parameters for the decreasing K tests used for the three CTSs tested are ω (Hz) = 30 Hz, R = 0.1 and $\Delta K_{máx} = 15$.

2.4 Scanning Electron Microscopy (SEM) and chemical composition

For the morphology analysis, a microscopy procedure was conducted on the samples resulting from the mechanical fracture test. The equipment used was a JEOL JSM 6610 Scanning Electron Microscope with a 30 kV acceleration voltage, 3nm resolution, and up to 300k X magnification capability with an EDS X-ray microanalysis system. The samples were analyzed under vacuum without prior chemical treatment, and the images were captured at 400X magnification in both the ductile fracture zone and the brittle fracture zone for two specimens previously selected. As the ductile/brittle transition zone was not precisely defined during the fracture tests, the images of each CTS were taken at stages II and III of the respective da/dN versus ΔK curves.

2.5 Micrographic analysis

A micrographic analysis was conducted to characterize the morphology and distribution of graphite nodules on the samples, utilizing an optical microscope with 40X magnification equipped with a 5-megapixel camera. The aspect ratio, roundness, and nodularity were measured and classified according to ISO 16112:2006 standard values of roundness. This procedure was performed on both the brittle and ductile fracture regions of each specimen. Additionally, another investigation was undertaken to determine the existence of a transition in the morphology and distribution of graphite nodules due to the cooling process. The transition zone between brittle and ductile fracture was identified through visual inspection aided by microscopic analysis.

3. Experimental results

3.1 Tensile tests

Tensile tests were conducted, and the stress versus strain curve is depicted in Fig. 2. Mechanical properties, including yield stress($\sigma_{0.2}$), ultimate stress, Young's modulus(E), and Poisson's ratio (ν), were obtained from the experimental curve and are reported in Table 1. These values represent the average of four tests. They were compared with values reported in the literature (Warda, 1990; Burditt, 1992) as referenced by [38].

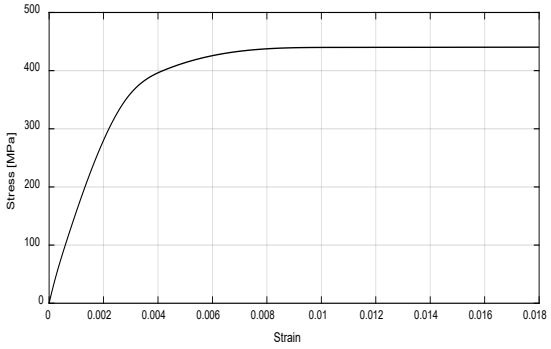

Figure 2. Stress-strain behavior of NCI determined from a tensile test. Source: Own elaboration

Table 1.
Experimental results from the tensile test.

Tensile test		
Yield stress $\sigma_{0.2}$ [MPa]	**Ultimate tensile stress σ_u [MPa]**	**Young's modulus E [GPa]**
325	437	171

Source: Own elaboration

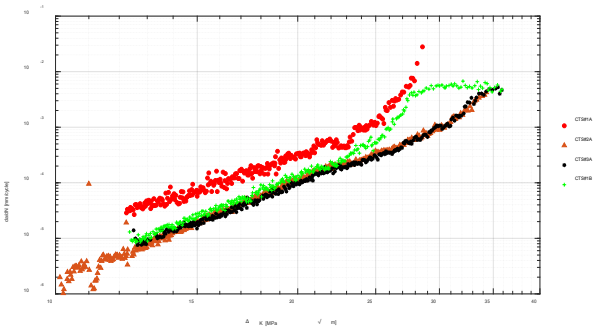

Figure 3. Comparison of da/dN vs ΔK curves (CTS #1A, #2A, #3A and #1B). Source: Own elaboration

3.2 Crescent K crack growth tests

As mentioned in section 2.3.1, "Investigation of crack propagation behavior in nodular cast iron based on its microstructure," in this part of the tests, a constant loading range with increasing K was applied to each of the four CTSs tested (CTS #1A, #2A, #3A, and #1B). Utilizing the "MTS Fatigue Crack Growth Test Ware" software of the MTS 810 machine, parameter values of the da/dN versus ΔK curves for each CTS, especially for stages II and III of the curves, were obtained. All curves obtained in this part of the tests are depicted in Fig.3.

Sample CTS #1A exhibits a curve that differs from the others obtained in this type of test due to its slope and higher crack propagation rate. Despite being part of the same batch as CTS #2A, #3A, and #1B samples, it's important to note that its direction and position in the original block differ (see Fig.1 a). Therefore, there's a possibility that the influence of graphite distribution in the crack direction may be more pronounced in CTS #1A than in the others. This could explain why the CTS #1A sample exhibited conditions conducive to greater crack growth acceleration with fewer cycles performed. With the CTS #2A specimen, the curve behavior was tested by decreasing the applied load by approximately 20%, from 7.94kN to 6.55kN, in order to provide a longer representation of the da/dN curve and a greater number of cycles. Despite the load decrease while maintaining the loading ratio (R) at 0.1, the curve's behavior remained largely unchanged compared to the others. A very similar behavior for the curves obtained in CTS samples #2A, #3A, and #1B can be observed. There is no significant dispersion in the points forming the curves or a large variation in their tendency, indicating that factors such as graphite nodules distribution did not significantly influence crack propagation acceleration or change in crack direction.

Table 2.
Results of increasing K tests.

CTS	N_f	a_c	ΔK_c	$Cx10^{-12}$	*m*
CTC#1	456783	27,76	28,58	190,6	4,76
CTS#2A	288647	35,47	34,32	0,7994	6,27
CTS#3A	824411	34,47	35,87	6,259	5,52
CTS#1B	809397	32,78	35,89	4,609	5,73

Source: Own elaboration

Some slightly scattered points regarding CTS #2A and #1B may be observed due to possible clip gauge displacements when the MTS 810 machine starts executing the cycles during the tests (see Fig. 4). Additionally, the similarity between the curves obtained for CTS #3A and CTS #1B is notable, forming practically one single curve. By checking Figure 1a, it can be seen that both specimens were taken from the bottom of the block but at opposite positions. From each generated curve, parameters related to stages II and III were calculated, allowing for the determination of critical stress intensity factor differential (ΔK_C), crack length (a_c), and constants of the Paris equation (C and m), as well as fatigue life calculation ($N_f - cycles$) for each CTS. Table 2 presents the results of the evaluated parameters $a_c(mm)$, $\Delta K_c(MPa\sqrt{m})$, C $\left(mm/cycle/MPa\sqrt{m}^{m}\right)$ and m, for each curve.

The parameters a_c, ΔK_c, C and m for samples CTS #2A, #3A, and #1B are very close to each other, with the values of C and m being closest to those reported in the literature. It is worth noting that the values for C and m parameters are characteristic of each material, and for the evaluated NCI, there is no clearly defined range. Therefore, the analysis of these parameters, in this case, is primarily based on the proximity of the results, which are satisfactorily consistent. The results of CTS #1A deviate significantly from most of the results obtained with the other specimens, as mentioned in the explanation of Fig. 1a. According to Table 4, sample CTS #1A exhibits a much smaller number of final cycles (N_f) compared to the other samples, resulting in smaller values of a_c and ΔK_c. However, similar to the other samples, the value for ΔK_c is very close to the value of ΔK_{IC} of 30 MPa$\sqrt{m}$ indicated by the DIN EN 1563 standard for an NCI GGG-40.

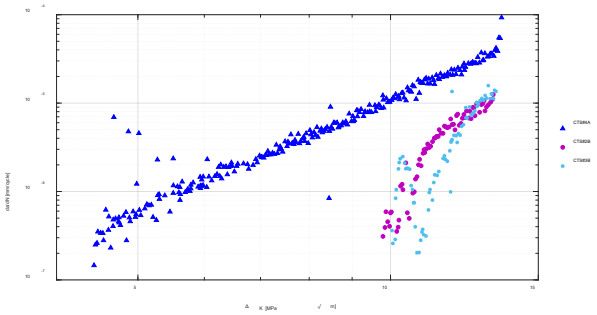

Figure 4. da/dN vs ΔK curve for CTS #4A, #2B and #3B.
Source: Own elaboration

3.3 *Decreasing K crack growth tests for stages II and III*

For this part of the tests, the procedure outlined in section 2.3.2, "Decreasing K test," was followed. The tests were conducted on three specimens, namely CTS #4A, #2B, and #3B. Utilizing the "MTS Fatigue Crack Growth Test Ware" software of the MTS 810 machine, parameter values of da/dN versus ΔK curves for each CTS at Stage I were obtained, as depicted in Fig.5.

In Fig. 4, it can be observed that the curve for the CTS #4A sample exhibits a steeper slope compared to those of the CTS #2B and #3B samples. In this scenario, it is probable that a similar phenomenon to that observed in the CTS #1A sample during the increasing K tests occurred, where despite having the same loading conditions as the other samples, there is a potential difference in the distribution of graphite nodules concerning the direction of crack growth. Such compositional disparity renders the behavior of the specimen more fragile than others, resulting in increased crack growth and a substantial decrease in K to a very small ΔK_{th} compared to other values obtained. The curves for the CTS #2B and #3B samples exhibit similar slopes and very close crack propagation rates. Conversely, the curve obtained for the CTS #4A sample indicates a lower crack propagation rate and a larger ΔK_{th} closer to the values found in the literature. These curves depict the anticipated behavior for a GGG-40 NCI with a more homogeneous distribution of graphite nodules and a structure characterized by a ferritic-pearlitic matrix. By comparing the three curves (CTS #4A, #2B, and #3B) shown in Fig. 5, the behavior of crack growth rates for each sample in Stage I can be observed more clearly. The results obtained for parameters such as the stress intensity factor threshold (ΔK_{th}), corresponding to Stage I of the da/dN versus ΔK curve, are presented in Table 3.

The results presented in Table 3 confirm the observations from Fig. 4. The discrepancy in cycle numbers can be attributed to the control method employed in the test, where each test was conducted until minimal or almost zero crack size variation was detected. Notably, crack propagation stabilized more rapidly in the CTS #3B sample. The crack sizes (a) were very similar for the CTS #2B and CTS #3B samples, indicating a closely matched behavior in terms of crack growth rates and corresponding ΔK_{th} values. This aligns with values suggested in the literature by some authors such as [39,40]. However, in the case of CTS #4A, a larger crack size (a) and a significantly smaller ΔK_{th} compared to the others are observed. Although this ΔK_{th} value is not drastically different from values reported by authors such as [41]. By examining the graphs obtained (Fig. 4 and Fig. 5), it was possible to combine and compare the different curves to observe the complete curve with all stages (I, II, and III) and obtain more comprehensive information about the general behavior of the material, as evaluated according to the parameters defined for each test. Fig. 6 presents the graphs obtained after comparing the da/dN versus ΔK curves for stages I, II, and III of each specimen.

Table 3.
Results of decreasing K tests.

CTS	N_f **(Ciclos)**	a (mm)	ΔK_{th} **(MPa** $\sqrt{m}$**)**
CTS #4A	9.229.601	26,37	4,35
CTS #2B	11.669.033	17,21	10,03
CTS #3B	3.807.131	17,37	11,68

Source: Own elaboration

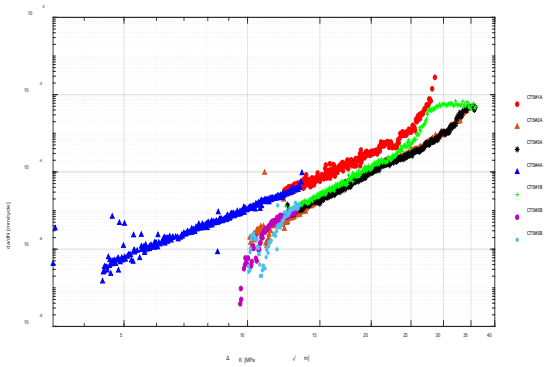

Figure 5. Comparison of complete da/dN vs ΔK curves.
Source: Own elaboration

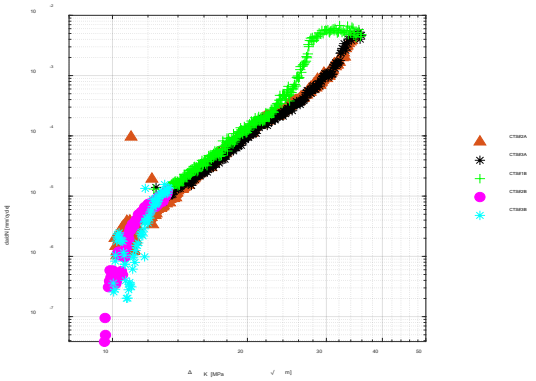

Figure 6. da/dN vs ΔK curve for CTS #2A, #3A, #1B, #2B and #3B.
Source: Own elaboration

From Fig.5, two sets of curves are discernible. The first set combines results from increasing K tests for specimens CTS #2A, #3A, #1B, and decreasing K for CTS #2B and #3B, exhibiting similar trends. These curves are presented in more detail in Fig. 6. The second set includes results for specimens CTS #1A (rising K) and CTS #4A (decreasing K), demonstrating a different tendency and slope compared to most of the CTS tested. This set is further discussed with the assistance of Fig. 8. Fig 7, displays curves with ΔK values consistent with theoretical values found in the literature (Section 2.2.2), where there is an average value of $\Delta K_{th} = 10{,}85\ MPa\sqrt{m}$ and an average value of $\Delta K_c = 34{,}24\ MPa\sqrt{m}$. These curves best depict the expected behavior for the chosen NCI in the tests' development.

On the other hand, the curve shown in Fig. 8 displays ΔK values that are not entirely characteristic of NCI. While the value of $\Delta K_c = 28{,}58\ MPa\sqrt{m}$ falls within parameters found in the literature, the value of $\Delta K_{th} = 4{,}35\ MPa\sqrt{m}$ is excessively low and does not align with characteristic values of the tested material. This suggests increased brittleness in a material that typically exhibits slightly more ductile behavior regarding crack growth, indicating a potential influence of graphite nodules specifically on these samples in accelerating crack propagation.

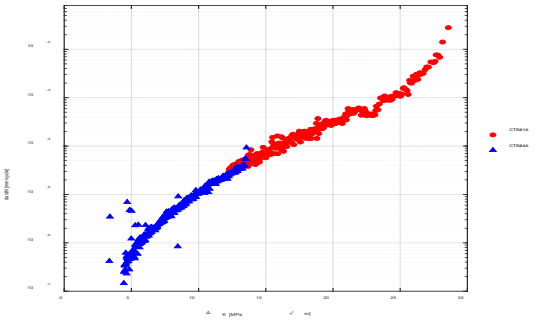

Figure 7. da/dN vs ΔK curve for CTS #1A, #4A.
Source: Own elaboration

Table 4.
The chemical composition of NCI (wt. %).

C	Mg	Si	P	S	Cr	Mn	Ni	Cu	Fe
3.6	0.08	2.52	0.06	0.02	0.07	0.41	0.31	0.06	92.87

Source: Own elaboration

3.4 Results and discussion of SEM analysis

The chemical compounds were measured by SEM-EDX equipment (JEOL JSM 6610 SEM-EDX, Musashino, Tokyo, Japan) and the results are presented in Table 4.

The present chemical composition aligns with the percentages reported by other authors [14,34,42]. The most significant elements (Fe, Si, and C), measured using SEM-EDX equipment, also demonstrate good agreement with the information provided by the casting company from which the samples were procured. In the casting process, additional elements such as silicon and magnesium are essential for modifying the solidification mechanism, while chromium contributes to enhancing tensile strength. According to [21], silicon stabilizes graphite, and magnesium facilitates nodule formation. The morphology and distribution of graphite nodules in nodular cast irons largely determine the mechanical response of the composite microstructures. The high carbon content is responsible for nodular graphite formation, with any remaining carbon contributing to the formation of lamellar perlite during nucleation. The difference observed in the da/dN versus ΔK curve for CTS #1A compared to the others prompted SEM analysis to investigate the morphology of graphite nodules and fracture appearance. The CTS #1A sample, sourced from the top of the NCI block, exhibited a more pronounced influence of graphite nodules on crack propagation, as indicated by the corresponding curve in Fig. 6. During the cooling process, graphite tends to float and nucleate near the top of the block, explaining the steeper slope and higher crack growth rate observed in the da/dN versus ΔK curve, which significantly differs from the other curves. Fig. 8 illustrates the regions where SEM images were captured. In this instance, images were taken at positions correlated with Stages II and III of the da/dN versus ΔK curves for CTS #1A and CTS #2A to facilitate comparison.

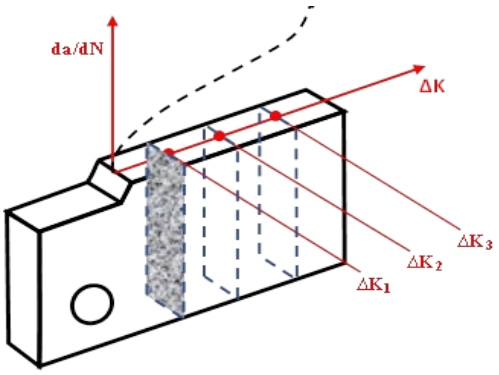

Figure 8. Scheme presenting the position where the images were taken by using SEM.
Source: Own elaboration

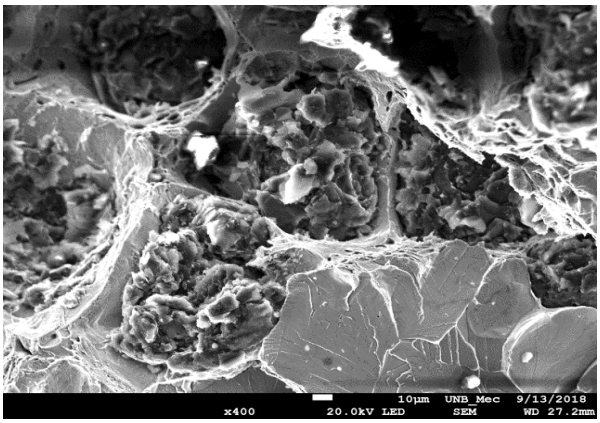

Figure 9. Sample CTS # 1A, a) fracture as stage II and b) fracture at stage III.
Source: Own elaboration

3.4.1 Sample CTS # 1A

Comparing the images obtained in Stage II (Fig. 9 a) and Stage III (Fig. 9 b) for CTS #1A at ×400 magnification, both ductile and brittle fracture mechanisms are observable. In Fig 9a), intercrystalline cleavage with the presence of coalescence is evident. Microvoids, resulting from plastic deformation induced by cyclic loading (microplasticity), are generally observed, highlighting ductile fracture characteristics. According to [7], portions of the matrix, particularly those surrounding graphite inclusions, undergo plastic deformation during ductile fracture. In contrast, Stage III (Fig 9b) displays transgranular cleavage, with the absence of coalescence and graphite nodules maintaining their complete shape. Transgranular cleavage fracture entails rapid crack propagation along specific crystallographic planes [43]. These planes typically exhibit the lowest packing density, requiring fewer bond breakages and greater spacing between planes. For many engineering metals, especially ferritic-pearlitic steels, cleavage represents the predominant mechanism of brittle failure, aligning well with the findings presented herein.

3.4.2 Sample CTS #2A

The morphology of the CTS #2A sample is depicted in Fig. 10. In Fig. 10 a), intergranular cleavage marks and some incomplete graphite nodules are visible, likely resulting from wear during the crack propagation process. This image also shows a significant presence of microvoids, indicating coalescence. The presence of coalescences is attributed to the ferritic-pearlitic composition of the microstructure, which facilitates intercrystalline cleavage and the formation of microvoids near the graphite nodules. Fig. 10.b) illustrates the flat surface (brittle fracture) where transgranular fracture mechanisms are evident. In this case, transgranular cleavage occurs, accompanied by nodules approximately 50µm in size, and there is an absence of the coalescence process.

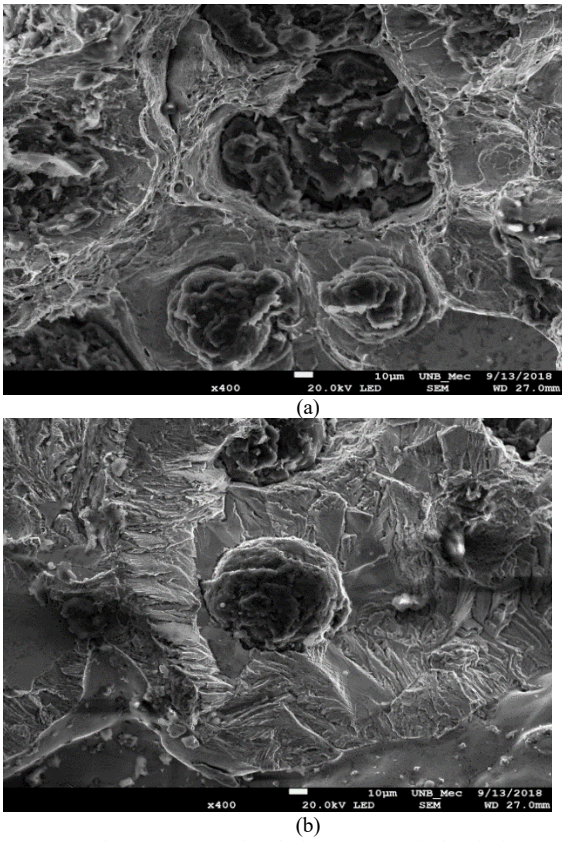

Figure10. Sample CTS #2A: a) ductile fracture zone. b) brittle fracture zone.
Source: Own elaborationMicrographic Analysis

A micrographic analysis was conducted to characterize the morphology and distribution of graphite nodules on the samples. This analysis utilized an optical microscope with 40x magnification equipped with a 5-megapixel camera. The aspect ratio (AR) was determined using Equation (1).

$$AR = \frac{major\ axis}{minor\ axis} \quad (1)$$

The roundness (Rd) is given by equation (2),

$$Rd = \frac{4A}{\pi L_m^2} \quad (2)$$

Where A is the area of the graphite and L_m is the Max feret of the graphite feature. The nodularity (Nd) is determined according to equation (3).

$$Nd = \left(\frac{\sum A_{nodular} + 0{,}5\sum A_{intermed}}{\sum A_{all}}\right) \times 100 \quad (3)$$

According to the ISO 16112:2006 standard, graphite nodules are classified based on their Rd. Nodules with Rd below 0.525 are categorized as graphite compacted, those falling within the range of 0.525 to 0.625 are classified as intermediate, and nodules with Rd values exceeding 0.625 are considered nodular. The results of the micrographic analysis are summarized in Table 5.

According to Table 5, CTS #1A exhibited a significantly higher fraction of graphite compared to the remaining samples. Additionally, it is evident that CTS #1A also had a lower quantity of nodules per unit of area, particularly noticeable in the ductile zone. This phenomenon can be attributed to the timing of nucleation and growth of graphite nodules. As noted by [21], magnesium acts as nuclei for graphite, initiating and facilitating its growth into spheroids. Nodules typically begin nucleating at around 1130°C, and the cooling rate during solidification controls their growth size. Higher cooling rates tend to result in smaller graphite growth compared to lower cooling rates. In the case of CTS #1A, the cooling rate may have accelerated graphite growth compared to the other CTS samples (CTS #2A, CTS #3A, and CTS #1B). Considering that all CTS samples originate from the same batch, it is reasonable to associate the position of each CTS within the block with irregularities in grain growth. The sensitivity of cooling speed during graphite nucleation in the

Table 5.
Experimental results obtained from the micrographics analysis.

CTS#	*Zone*	*qd*	*%área*	*Nod.size*	*AR*	*Rd*	*Nd*
1A	II	31,40	24,98	63,66	1,479	0,726	85,48
2A		20,40	13,35	57,72	1,525	0,714	79,34
3A		43,60	9,29	32,94	1,779	0,727	90,96
1B		38,00	9,82	36,28	1,495	0,728	85,56
1A	III	20,00	23,84	77,92	1,648	0,673	89,24
2A		42,60	13,60	40,33	1,564	0,705	85,89
3A		30,80	8,35	37,15	1,602	0,703	88,86
1B		44,20	8,35	31,01	1,597	0,697	83,09

Source: Own elaboration

NCI manufacturing process is underscored by the findings presented here. Additionally, apart from graphite solidification, several factors contribute to poor aspect ratios and nodularity observed in the graphite nodules of CTS #1A. These factors may include low residual magnesium, ineffective post-inoculation due to silicon excess, presence of high levels of tramp elements, or carbonaceous residues leading to the deterioration of spheroidal graphite. Numerous studies have indicated that nodularity reductions, even within ferritic, pearlitic, or ferritic-pearlitic matrices, result in decreased tensile and impact properties. The mechanical properties are inversely proportional to nodularity levels, with decreasing nodularity correlating with reduced fatigue strength and affecting crack propagation. Finally, the present findings align well with the work of [24], where they asserted that an increase in non-spheroidal graphite content in pearlitic or ferritic steel leads to a progressive decrease in fatigue limit.

4. Final conclusions

Due to their appealing properties, nodular cast irons (NCIs) are widely employed in various components across industries such as automotive, aerospace, and energy. The present study aims to deepen the understanding of a specific batch of NCI by incorporating fatigue crack growth investigations into a series of previously conducted tests and studies. This research endeavors to explore potential correlations between crack propagation behavior and microstructural morphology, particularly focusing on the NCI alloy GGG40. Preliminary conclusions drawn from the crack propagation tests and microstructural analysis are outlined herein. The microstructural examination confirms the typical morphology observed in NCI alloys, characterized by graphite spheroids or nodules dispersed within a ferritic matrix. The distribution and size of these graphite nodules in the NCI microstructure align with the mechanical properties observed in the tested samples. It is widely acknowledged that NCI materials exhibit a broad range of mechanical properties, attributed to the distribution and morphology of graphite nodules. Notably, even specimens sourced from the same NCI block demonstrate discernible differences in crack propagation properties, highlighting the significant influence of graphite nodule distribution. Specimens extracted from the top of the NCI block exhibited higher crack propagation rates. For comprehensive analysis, the fractured specimens were categorized into brittle and ductile regions on their surfaces. Subsequent SEM analysis was conducted on each region to examine fracture patterns and morphology. In specimens originating from the top of the NCI block, the influence of nodular graphite was observed, attributed to the flotation mechanism. Micrographic analysis was employed to determine the size, roundness, shape, and distribution of graphite nodules. Previous research has indicated that graphite nodule flotation occurs due to excessive growth of certain nodules, which absorb carbon directly from the liquid phase. Due to their lower density, these graphite nodules tend to migrate towards the surface. This phenomenon likely explains the variation in fracture behavior observed based on the specimen's position within the NCI block. Further

investigation is warranted to validate these preliminary findings and advance understanding of fatigue and fracture behavior in the specific NCI alloy examined in this study. Specifically, exploring the influence of stress ratio (R), the presence of overloads in variable amplitude loading histories, and delving into more detailed fracture mechanisms would be fruitful avenues for future research.

Acknowledgments

This research was supported by FAPDF (Research Foundation of Federal District) project number 0193.001554/2017 and CNPq (National Council for Scientific and Technological Development) project number 408551/2016-0 and 314602/2021-6. The first author expresses gratitude to the National Council for Scientific and Technological Development (CNPq) for providing the fellowship grant with reference number 314602/2021-6. The first also thank to the Foundation for Research Support of the Federal District (FAPDF), Process No. 00193-00002184/2023-91.

Bibliography

[1] Labrecque, C., and Gagné, M., Ductile Iron: fifty years of continuous development, Can. Metall. Q. 37(5), pp. 343–378, 1998. DOI: https://doi.10.1179/cmq.1998.37.5.343.

[2] Hervas, I., Ben-Bettaieb, M., Thuault, A., and Hug, E., Graphite nodule morphology as an indicator of the local complex strain state in ductile cast iron, Materials & Design, 52, pp. 524-532, 2013. DOI: https://doi.org/10.1016/j.matdes.2013.05.078

[3] Di-Cocco,V., Iacoviello, F., Rossi, A., and Ecarla, F., Mechanical properties gradient in graphite nodules:influence on ferritic DCI damaging micromechanisms, 2013, pp. 222–230.

[4] Iacoviello, F., Di-Bartolomeo O., Di-Cocco, V. and Piacente, V., Damaging micromechanisms in ferritic-pearlitic ductile cast irons, Mater. Sci. Eng. A, 478(1–2), pp. 181–186, 2008. DOI: https://doi.org/10.1016/j.msea.2007.05.110.

[5] Bonora N., and Ruggiero, A., Micromechanical modeling of ductile cast iron incorporating damage. part I: ferritic ductile cast iron, Int. J. Solids Struct., 42(5–6), pp. 1401–1424, 2005. DOI: https://doi.org/10.1016/j.ijsolstr.2004.07.025.

[6] Lacaze, J., Solidification of spheroidal graphite cast irons: III. Microsegregation related effects, Acta Mater., 47(14), pp. 3779–3792, 1999. DOI: https://doi.org/10.1016/S1359-6454(99)00233-5.

[7] Fernandino, D.O., and Boeri, R., Study of the fracture of ferritic ductile cast iron under different loading conditions, Fatigue Fract. Eng. Mater. Struct., 38(5), pp. 610–620, 2015. DOI: https://doi.org/10.1111/ffe.12266.

[8] Ceschini, L., Morri, A., and Morri, A., Effects of casting size on microstructure and mechanical properties of spheroidal and compacted graphite cast irons: experimental results and comparison with international standards, J. Mater. Eng. Perform., 26(6), pp. 2583–2592, 2017. DOI: https://doi.org/10.1007/s11665-017-2714-7.

[9] Queirós, R., Domeij, B., and Diószegi, A., Unraveling compacted and nodular cast iron porosity: case studies approach, Inter Metalcast., 18, pp. 1811–1830, 2024. DOI: https://doi.org/10.1007/s40962-023-01149-9

[10] Xu, M.S., and Shi, J.L., Fracture analysis of nodular cast iron crankshaft, Metalurgija, 59(4), pp. 517–520, 2020.

[11] Betancur, A., Anflor, C., Pereira, A., and Leiderman, R., Determination of the effective elastic modulus for nodular cast iron using the boundary element method, Metals (Basel), 8(8), art. 641, 2018. DOI: https://doi.org/10.3390/met8080641.

[12] Hütter, G., Zybell, L., and Kuna, M., Micromechanisms of fracture in nodular cast iron: From experimental findings towards modeling strategies. A review, Eng. Fract. Mech., 144(6), pp. 118–141, 2015. DOI: https://doi.org/10.1016/j.engfracmech.2015.06.042.

[13] Iacoviello, F., Di-Cocco, V., Rossi, A., and Cavallini, M., Ferritic-pearlitic ductile cast irons: Is ΔK a useful parameter? 13th Int. Conf. Fract. 2013, ICF 2013, 2, 2013, pp. 998–1006.

[14] Vaško, A., and Chalupová, M., The micro-mechanisms of failure of nodular cast iron, Prod. Eng. Arch., 5(4), pp. 31–35, 2014.

[15] Hütter, G., Zybell, L., and Kuna, M., Micromechanisms of fracture in nodular cast iron: From experimental findings towards modeling strategies - A review, Eng. Fract. Mech., 144, pp. 118–141, 2015. DOI: https://doi.org/10.1016/j.engfracmech.2015.06.042.

[16] Gonzaga, R.A., Influence of ferrite and pearlite content on mechanical properties of ductile cast irons, Mater. Sci. Eng. A, 567, pp. 1–8, 2013. DOI: https://doi.org/10.1016/j.msea.2012.12.089.

[17] Costa, N., Machado, N., and Silva, F.S., A new method for prediction of nodular cast iron fatigue limit, Int. J. Fatigue, 32(7), pp. 988–995, 2010. DOI: https://doi.org/10.1016/j.ijfatigue.2009.11.005.

[18] Čanžar, P., Tonkovich, Z., and Kodvanj, J., Microstructure influence on fatigue behaviour of nodular cast iron, Mater. Sci. Eng. A, 556, pp. 88–99, 2012. DOI: https://doi.org/10.1016/j.msea.2012.06.062.

[19] Ferro, P., Lazzarin, P., and Berto, F., Fatigue properties of ductile cast iron containing chunky graphite, Mater. Sci. Eng. A., 554, pp. 122–128, 2012. DOI: https://doi.org/10.1016/j.msea.2012.06.024.

[20] Nan, L., Shu ming, X., and Pei-wei, B., Microstructure and mechanical properties of nodular cast iron produced by melted metal die forging process. J. Iron Steel Res. Int., 20(6), pp. 58–62, 2013. DOI: https://doi.org/10.1016/S1006-706X(13)60112-0

[21] Azeem, M.A., Bjerre, M.K.R., Atwood, C., Tiedje, N., and P.D. Lee, Synchrotron quantification of graphite nodule evolution during the solidification of cast iron, Acta Mater., 155, pp. 393–401, 2018. DOI: https://doi.org/10.1016/j.actamat.2018.06.007.

[22] Escobar, A., Celentano, D., Cruchaga, M., and Schulz, B., On the effect of pouring temperature on spheroidal graphite cast iron solidification, Metals (Basel)., 5(2), pp. 628–647, 2015. DOI: https://doi.org/10.3390/met5020628.

[23] Lucas, L., Boneti, T.M., Hupalo, S.F., Junior, V., and Rosário, A.M., Influence of casting heterogeneities on microstructure and mechanical properties of austempered ductile iron (ADI), No. Stage II, 2017.

[24] Voigt R.C., and Loper, C.R., Austempered ductile iron - process control and quality assurance, J. Mater. Eng. Perform., 22(10), pp. 2776–2794, 2013. DOI: https://doi.org/10.1007/s11665-013-0712-y.

[25] Dong, M.J., Prioul, C., and Francois, D., Damage effect on the fracture toughness of nodular cast iron: Part I. Damage characterization and plastic flow stress modeling, Metall. Mater. Trans. A Phys. Metall. Mater. Sci., 28(11), pp. 2245–2254, 1997. DOI: https://doi.org/10.1007/s11661-997-0182-7

[26] Berdin, C., Dong, M.J., and Prioul, C., Local approach of damage and fracture toughness for nodular cast iron, Engineering Fracture Mechanics, 68(9), pp. 1107–1117, 2001. DOI: https://doi.org/10.1016/S0013-7944(01)00010-8

[27] Vaško, A., Hurtalová, L., Uhríčik, M., and Tillová, E., Fatigue of nodular cast iron at high frequency loading, Materwiss. Werksttech., 47(5–6), pp. 436–443, 2016. DOI: https://doi.org/10.1002/mawe.201600519

[28] Ulewicz R., and Tomski, P.S., The effect of high-frequencies loading on the fatigue cracking of nodular cast iron, 2019, pp. 5–7.

[29] Seleš, K., Tomić, Z., and Tonković, Z., Microcrack propagation under monotonic and cyclic loading conditions using generalised phase-field formulation, Eng. Fract. Mech., 255, art. 107973, 2021. DOI: https://doi.org/10.1016/j.engfracmech.2021.107973.

[30] D'-Agostino, L., De-Santis, A., Di-Cocco, V., Iacoviello, D., and Iacoviello, F., Fatigue crack propagation in Ductile Cast Irons: an Artificial Neural Networks based model, Procedia Struct. Integr., 3, pp. 291–298, 2017. DOI: https://doi.org/10.1016/j.prostr.2017.04.048

[31] Di-Cocco, V., Iacoviello, F., and Cavallini, M., Damaging micromechanisms characterization of a ferritic ductile cast iron, Eng. Fract. Mech., 77(11), pp. 2016–2023, 2010. DOI: https://doi.org/10.1016/j.engfracmech.2010.03.037

[32] Iacoviello, F., and Di-Cocco, V., Ductile cast irons: microstructure influence on fatigue crack propagation resistance, Frat. Ed Integrità Strutt., 13(13), pp. 3–16, 2010. DOI: https://doi.org710.3221/IGF-ESIS.13.01

[33] Di-Cocco, V., Iacoviello, F., Rossi, A., Cavallini, M., and Natali, S., Graphite nodules and fatigue crack propagation micromechanisms in a ferritic ductile cast iron, Fatigue Fract. Eng. Mater. Struct., 36(9), pp. 893–902, 2013. DOI: https://doi.org/10.1111/ffe.12056
[34] Iacoviello F., and Di Cocco, V., Influence of the graphite elements morphology on the fatigue crack propagation mechanisms in a ferritic ductile cast iron, Eng. Fract. Mech, 167, pp. 248–258, 2016. DOI: https://doi.org/10.1016/j.engfracmech.2016.03.041
[35] Limodin N., et al., Influence of closure on the 3D propagation of fatigue cracks in a nodular cast iron investigated by X-ray tomography and 3D volume correlation, Acta Mater., 58(8), pp. 2957–2967, 2010. DOI: https://doi.org/10.1016/j.actamat.2010.01.024
[36] Betancur A., and Anflor, C.T.M., Multi-Scaling homogenization process for nodular cast iron using BEM, J. Multiscale Model., 08(03n04), art. 1740005, 2017. DOI: https://doi.org/10.1142/s1756973717400054
[37] Pereira, A., Costa, M., Anflor, C., Pardal, J., and Leiderman, R., Estimating the effective elastic parameters of nodular cast iron from micro-tomographic imaging and multiscale finite elements: comparison between numerical and experimental results, Metals, 8(9), art. 695, 2018. DOI: https://doi.org/10.3390/met8090695
[38] Fernandino, D.O., Cisilino, A.P., and Boeri, R.E., Determination of effective elastic properties of ferritic ductile cast iron by computational homogenization, micrographs and microindentation tests, Mech. Mater., 83, pp. 110–121, 2015. DOI: https://doi.org/10.1016/j.mechmat.2015.01.002
[39] Mottitschka, T., Pusch, G., Biermann, H., Zybell, L., and Kuna, M., Influence of overloads on the fatigue crack growth in nodular cast iron: Experiments and numerical simulation, Procedia Eng. 2(1), pp. 1557–1567, 2010. DOI: https://doi.org/10.1016/j.proeng.2010.03.168
[40] Dahlberg, M., Fatigue crack propagation in nodular graphite cast iron. International Journal of Cast Metals Research, 17(1), pp. 29–37, 2004. DOI: https://doi.org/10.1179/136404604225012398
[41] Wasén, J., and Heier, E., Fatigue crack growth thresholds - The influence of Young's modulus and fracture surface roughness, Int. J. Fatigue, 20(10), pp. 737–742, 1998. DOI: https://doi.org/10.1016/S0142-1123(98)00034-6
[42] de Sousa, J.A.G., Sales, W.F., Guesser, W.L., and Machado, Á.R., Machinability of rectangular bars of nodular cast iron produced by continuous casting, Int. J. Adv. Manuf. Technol., 98(9–12), pp. 2505–2517, 2018. DOI: https://doi.org/10.1007/s00170-018-2387-x.
[43] Anderson, T.L., Fracture Mechanics: Fundamental and Applications. 2017.

C.T.M. Anflor, holds a BSc. Eng. in Mechanical Engineering in 2000, from the University of Passo Fundo. MSc. in Mechanical Engineering in 2003, from the Federal University of Rio Grande do Sul, and a PhD. in Mechanical Engineering in 2007, from the same university, with further doctoral research at Brunel University London, UK in 2013. She is currently a professor of Automotive Engineering at the University of Brasília. Her expertise includes mechanical vibrations, boundary element methods, and solid mechanics. Anflor is the leader of the Experimental and Computational Mechanics Group (GMEC) at the University of Brasília.
ORCID: 0000-0003-3941-8335

J. Hurtado-Águalimpia, holds a BSc. Eng. in in Civil Engineering in 2013, from the University of Antioquia, Colombia. MSc. in Engineering Materials Integrity. His research experience focuses on mechanical testing and the fracture/fatigue mechanics of engineering materials.
ORCID:0009-0001-1759-7881

A.A. Betancur-Arroyave, received his PhD. in Mechanical Sciences in 2017, from the University of Brasília and his MSc. in Chemical Engineering in 2012, from the Facultad de Minas, at the Universidad Nacional de Colombia. He is currently an instructor at SENAI-Brasília and active member of the Group of Experimental and Computational Mechanics (GMEC) at the University of Brasília. His research interests include materials science and computational mechanics.
ORCID: 0000-0002-6687-1197

S.H.S. Carneiro, holds a BSc. Eng. in Mechanical-Aeronautical Engineering in 1987, from the Instituto Tecnológico de Aeronáutica (ITA). MSc. in Aeronautical and Mechanical Engineering in 1993, with a focus on Structures, from ITA, and a PhD. in Engineering Mechanics in 2000 from the Virginia Polytechnic Institute and State University. He is currently an associate professor in the Aerospace Engineering program and active member of the Group of Experimental and Computational Mechanics (GMEC) at the University of Brasília.
ORCID: 0000-0001-6669-2255

J.N.V. Goulart, holds a BSc. Eng. in Civil Engineering in 1999, from the University of Passo Fundo, and both a MSc. and PhD. in Mechanical Engineering from the Federal University of Rio Grande do Sul, with a focus on transport phenomena and solid mechanics. He is currently a professor in the Energy Engineering program at the University of Brasília. He is also an affiliated faculty member of the Graduate Program in Engineering Materials Integrity (PPGIntegridade) and an active member of the Group of Experimental and Computational Mechanics (GMEC) at the University of Brasília.
ORCID: 0000-0002-3045-1975